



## Regression Model for the Mechanical Properties of PVC-P Geomembranes with Scratch Damage



Xianlei Zhang<sup>1\*</sup>, Jianqun Liu<sup>1</sup>, Wenhui Zhang<sup>2</sup>, Hesong Liu<sup>1</sup>

<sup>1</sup> School of Water Conservancy, North China University of Water Resources and Electric Power, 450045 Zhengzhou, China

<sup>2</sup> School of Information Engineering, North China University of Water Resources and Electric Power, 450045 Zhengzhou, China

\* Correspondence: Xianlei Zhang (zhangxianlei@ncwu.edu.cn)

Received: 11-12-2023

Revised: 12-20-2023

Accepted: 12-27-2023

**Citation:** X. L. Zhang, J. Q. Liu, W. H. Zhang, and H. S. Liu, "Regression model for the mechanical properties of PVC-P geomembranes with scratch damage," *J. Civ. Hydraul. Eng.*, vol. 1, no. 1, pp. 49–59, 2023. <https://doi.org/10.56578/jche010105>.



© 2023 by the authors. Published by Acadlore Publishing Services Limited, Hong Kong. This article is available for free download and can be reused and cited, provided that the original published version is credited, under the CC BY 4.0 license.

**Abstract:** In response to the mechanical performance alterations of PVC-P geomembranes due to improper handling or subgrade particle action during construction and operation, a series of axial tensile tests on PVC-P geomembranes with various scratch damages were conducted. Multifactorial variance analysis was performed using Python, and a multivariate regression model for the fracture strength and elongation at break of scratched PVC-P geomembranes was developed using SPSS. The precision of the regression model was evaluated using parameters such as the coefficient of determination ( $R^2$ ), mean absolute error (MAE), mean absolute percentage error (MAPE), and root mean square error (RMSE). The results indicated that the fracture strength and elongation at break of PVC-P geomembranes are significantly affected by a combination of scratch angle, length, and depth. The impact on elongation at break is greater than on fracture strength, with the scratch angle having the most significant effect. The developed multivariate regression model yielded  $R^2$  values of 0.98 and 0.97 for fracture strength and elongation at break, respectively. The MAEs were 0.62 kN/m and 7.96%, and the MAPEs were 3.06% and 5.13%, respectively. The RMSEs were 0.84 kN/m and 12.08%. The high fitting accuracy of the model suggests its utility for evaluating the mechanical performance of PVC-P geomembranes with scratch damage.

**Keywords:** PVC-P geomembrane; Scratch damage; Fracture strength; Elongation at break; Variance analysis; Multivariate regression

### 1 Introduction

PVC-P geomembranes, recognized for their low cost, strong adaptability to deformation, minimal climatic impact, and ease of construction, have been widely applied in impermeable projects such as reservoir dams, landfill sites, mining, and water conveyance tunnels [1–3]. According to the International Commission on Large Dams (2010), 86 out of 167 geomembrane-impermeable dams globally utilize PVC-P geomembranes [4]. In China, the use of geomembrane for impermeability began in the early 1980s, primarily in reinforcement projects [4], and later extended to new small and medium-sized hydropower projects [5], predominantly employing HDPE/PE geomembranes. Early 21st-century projects revealed mechanical deficiencies in HDPE/PE geomembranes, such as poor adaptability to differential deformation and excessive hardness in thicknesses over 1.0mm [6]. In contrast, PVC-P geomembranes with a thickness of no less than 2.5mm maintained superior flexibility, leading to their growing recognition and application in projects such as the VI Level of the Nam Ou River Cascade Hydropower Project and the Jiangpinghe Hydropower Stations. Extensive research by domestic scholars on the application of PVC-P geomembranes in face membrane rockfill dams has achieved significant progress [7, 8], with findings being utilized in high-face membrane rockfill dam impermeability projects [9].

During construction and operation, geomembranes are susceptible to structural damage from external disturbances, resulting in a decline in mechanical performance. Whether this meets the engineering design standards/specifications has been a subject of extensive research. Investigations by Gallagher et al. [10] into landfill integrity found geomembrane damage such as wrinkles, holes, and scratches, primarily caused by construction equipment or

techniques, but their focus was on holes and wrinkles, lacking precise mechanical analysis of scratch damage. Research by Giroud and Morel [11] derived relationships between various parameters of wrinkled geomembrane damage and external conditions, yet only considering horizontally based wrinkle shapes and not analyzing different wrinkle forms. Study by Narejo et al. [12] on long-term and short-term puncture tests of HDPE geomembranes proposed empirical formulas for top puncture, applicable only to HDPE geomembranes, offering limited guidance for other types. Stark et al. [13] conducted top puncture tests on PVC geomembranes, exploring relationships between top puncture height, force, and thickness, but failed to derive precise theoretical formulas. Research by Xu et al. [14] on folded and perforated geomembrane axial tensile mechanical properties indicated a significant reduction in the mechanical performance of damaged HDPE geomembranes, accurately analyzing the mechanical performance changes of HDPE geomembranes with different numbers and diameters of holes, yet no theoretical formulas linking mechanical performance to hole parameters were derived. Study by Rowe and Fan [15] on HDPE geomembranes with various sizes and shapes of defect holes in permeability tests concluded that the shape of the damaged hole is a major factor in increased permeability of the geomembrane, but did not analyze the permeability performance of HDPE geomembranes with scratch damage. Research by Cen et al. [16] on mechanical performance tests of HDPE geomembranes with pore-like, seam-like, and scratch-like damage found that defects and damage reduce mechanical performance; although the study analyzed the weakening of mechanical performance by scratch damage, it focused only on three depths of scratch damage, not considering the impact of different lengths and angles of scratch damage.

Due to improper laying methods during construction or the effect of sharp particles in the subgrade, PVC-P geomembranes can suffer scratch damage. Engineers cannot ascertain whether the mechanical performance degradation of scratched PVC-P geomembranes affects the safe operation of the project, with limited related experimental research and theoretical results available [17]. Thus, it is essential to thoroughly investigate the mechanical performance degradation patterns of PVC-P geomembranes with varying degrees of scratch damage. Regression analysis, a mathematical method used to establish relationships between independent and dependent variables and construct strong correlations [18], is widely applied in various fields [19, 20]. Based on the results of axial tensile tests of scratched PVC-P geomembranes, this paper constructs a multivariate regression model to predict the degree of mechanical performance degradation under different levels of scratch damage. This provides a reference for assessing the mechanical performance of scratched PVC-P geomembranes, drawing attention from construction engineers to the importance of scratch damage in PVC-P geomembranes and from design engineers to the quality requirements of projects.

## 2 Experimental Conditions

### 2.1 Test Materials

The test specimens were made from domestically produced PVC-P geomembrane using the calendering process. Each geomembrane roll was 45.0m long, 2.0m wide, and 2.0mm thick. The physical and mechanical properties are shown in Table 1.

**Table 1.** Main parameters of PVC-P geomembrane

Thickness /mm	Mass Per Unit Area / g · cm <sup>-2</sup>	Break Strength /kN · m <sup>-1</sup>	Elongation at Break / %
2.00	0.28	27.63	241.65

### 2.2 Test Scheme and Method

In accordance with the SL235-2012 *Specifications for Test and Measurement of Geosynthetics* [21], narrow strip specimens for axial tensile tests were selected. During sample preparation, the 100mm edge and any flawed or damaged parts of the entire geomembrane roll were discarded. Standard specimens were cut using a specially designed mold, with a gauge length of 100mm and a width of 50mm, as shown in subgraph (a) of Figure 1. The test temperature was set at 20±2°C, with a stretching rate of 10mm/min. The axial tensile testing instrument used was a universal testing machine for geosynthetic materials, with the following basic parameters: maximum load capacity of 30.0kN, maximum travel of 2.1m, deformation detection range from 0.2% to 100% of the maximum travel, and error range within ±0.5%. During the tensile test of the specimens, the two clamps were adjusted to 100mm to keep the specimen clamped and flat. The universal testing machine was started at the set rate until the specimen broke. The start and stop of the testing machine were controlled by a computer, and the test data were collected by professional data acquisition software at a frequency of 15.0Hz.

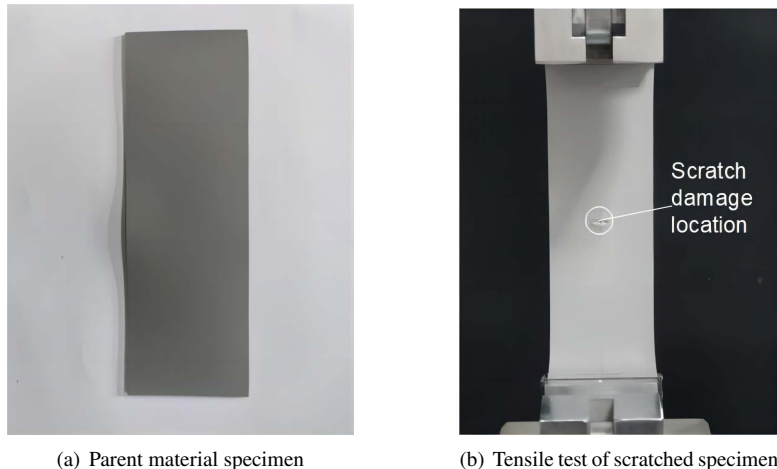


**Figure 1.** PVC-P geomembrane specimen diagram

The sample preparation equipment utilized for this experiment was a self-developed scratch sampler. This instrument is made from a 0.5mm-thick rectangular steel piece, with one end fashioned into a blade for creating scratch damage. When making the scratches, the blade is placed horizontally on the surface of the geomembrane specimen. The blade is marked with different depth scales to produce scratches of varying depths on the geomembrane. Additionally, the sampler has varying lengths corresponding to different scratch lengths. A protractor is used to measure and mark different scratch angles on the specimen. In this experiment, scratches of various angles, lengths, and depths were made in the central area of the standard specimen. To realistically reflect the different degrees of scratch damage that might occur in PVC-P geomembranes in engineering projects, the experiment was designed with a combination of seven scratch angles, seven scratch length ratios, and four scratch depth ratios. In subgraph (b) of Figure 1 shows a specimen with one such combination of scratch damage, with the marked area indicating the location of the scratch damage. The scratch angle, denoted as  $\alpha$ , is the angle between the direction of the scratch length and the axial tension direction, set at  $0^\circ, 15^\circ, 30^\circ, 45^\circ, 60^\circ, 75^\circ$ , and  $90^\circ$ . The damage length ratio, represented by  $\beta$ , is the ratio of the scratch length to the width of the specimen, set at 10%, 20%, 30%, 40%, 50%, 60%, and 80%, corresponding to scratch lengths of 5mm, 10mm, 15mm, 20mm, 25mm, 30mm, and 40mm, respectively. The scratch depth ratio, denoted as  $\gamma$ , is the ratio of the scratch depth to the thickness of the PVC-P geomembrane, set at 25%, 50%, 75%, and 100%, corresponding to scratch depths of 0.5mm, 1.0mm, 1.5mm, and 2.0mm, respectively. A total of 196 different combinations of scratch damage were tested in tensile tests. For each combination of scratch damage, five tests were conducted, yielding a total of 980 sets of test data.

### 2.3 Model Evaluation Metrics

To assess the accuracy of the regression model, statistical measures such as  $R^2$ , MAE, and MAPE are employed. The closer the  $R^2$  value is to 1, and the smaller the MAE and MAPE values are, the higher the accuracy of the model. The expressions for these metrics are as follows:

$$R^2 = \frac{\sum (\hat{y}_i - \bar{y})^2}{\sum (y_i - \bar{y})^2} \quad (1)$$

$$MAE = \frac{1}{n} \sum_{i=1}^n |y_i - \hat{y}| \quad (2)$$

$$MAPE = \frac{100\%}{n} \sum_{i=1}^n \left| \frac{y_i - \hat{y}}{y_i} \right| \quad (3)$$

where,  $\bar{y}$  represents the average value of the experimental data; %,  $\hat{y}_i$  is the model-predicted value for the  $i$ -th sample;  $y_i$  is the experimental value for the  $i$ -th sample; and  $n$  denotes the number of samples.

## 3 Preliminary Analysis of Experimental Results

### 3.1 Break Strength

The data were imported into the Origin 2018 software to create line charts for different combinations, as shown in Figures 2 and 3. Subgraph (a) of Figure 2 displays a three-dimensional scatter plot of the break strength ( $T$ ) of PVC-P

geomembranes with various combinations of scratch damage. It can be observed that the break strength of PVC-P geomembranes decreases to varying degrees with the increase in  $\alpha$  (scratch angle),  $\beta$  (scratch length ratio), and  $\gamma$  (scratch depth ratio). Subgraph (b) through Subgraph (e) of Figure 2 show the variation curves of break strength of PVC-P geomembranes with increasing  $\alpha$  under four different depth ratios. From Subgraph (b) of Figure 2, it is noted that when  $\gamma=25\%$ , the decrease in break strength with increasing  $\alpha$  is relatively minor for  $\beta$  values between 10%-30%. This could be due to the increased area of scratch damage as  $\beta$  increases, leading to a reduction in the effective tensile area of the geomembrane and hence a decrease in its mechanical properties. When  $\beta \geq 40\%$ , a more significant decrease in strength is observed. For  $\beta=40\%$  and 50%, the rate of decrease initially increases and then decreases with the angle, while for  $\beta=60\%-80\%$ , the rate of decrease gradually diminishes. At  $\gamma=50\%$ , the trend of decrease in break strength with increasing  $\alpha$  first increases and then decreases, with a reduction rate of 36.86% at  $\alpha=90^\circ$  for  $\beta=10\%$  and 70.21% for  $\beta=80\%$ . For  $\gamma=75\%$  and 100%, the rate of decrease gradually diminishes, and for  $\gamma$  values between 50%-100% and  $\alpha$  between 75-90°, the decrease in break strength is almost negligible. Taking  $\gamma=75\%$  and  $\beta=20\%$  as an example, the reduction rates compared to the parent material are 47.83% and 49.24% for  $\alpha=75^\circ$  and  $\alpha=90^\circ$ , respectively.

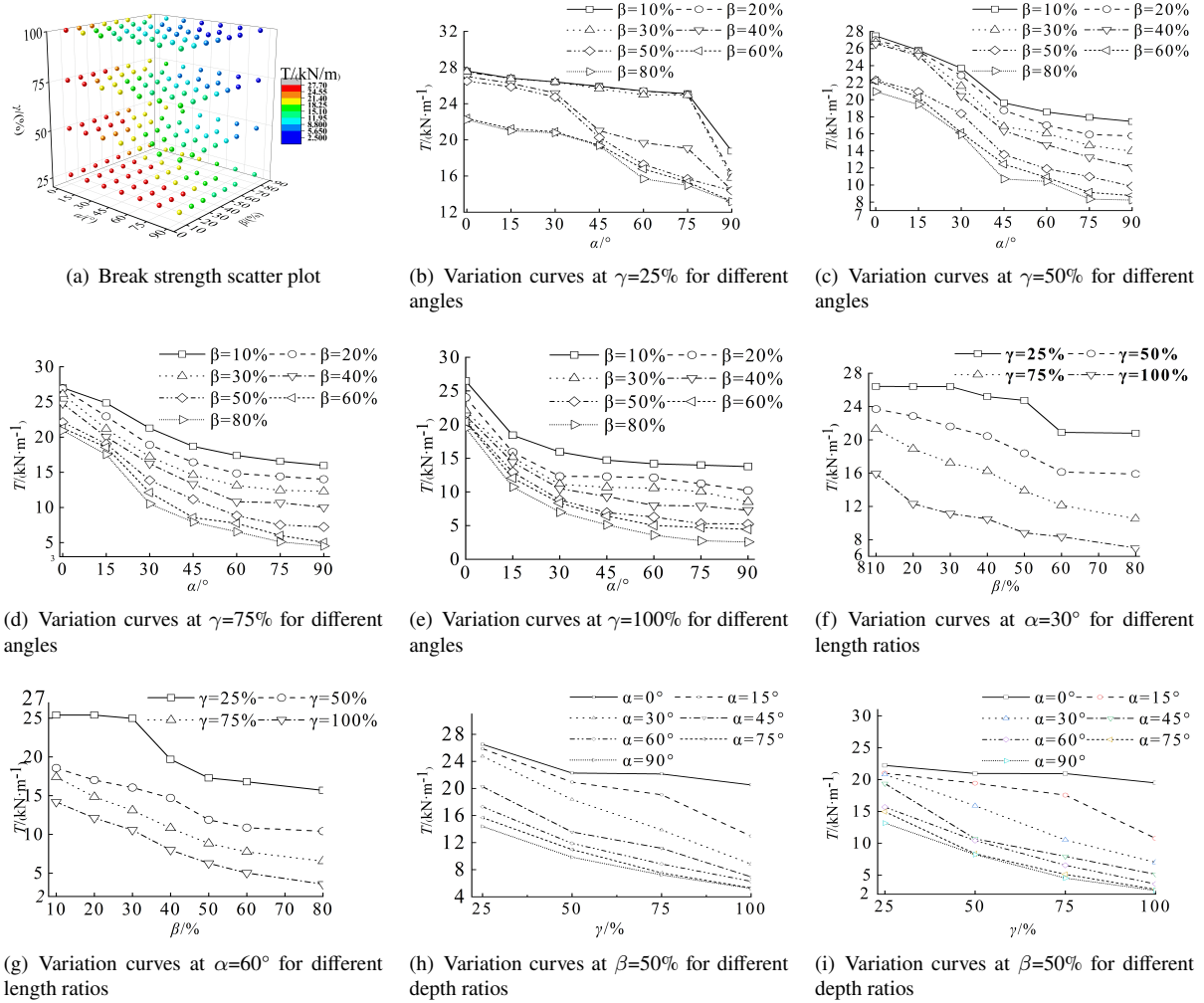


**Figure 2.** Variation of break strength

Subgraph (f) and Subgraph (g) of Figure 2 show the curves of break strength at  $\alpha=30^\circ$  and  $60^\circ$  for different length ratios. It is observed that at  $\gamma=25\%$ , the reduction in break strength with increasing  $\beta$  is significant, whereas the decrease for other  $\gamma$  values is less than that for  $\gamma=25\%$ , with a reduction rate of 43.21% at  $\alpha=60^\circ$  for  $\gamma=25\%$ . Subgraph (h) and Subgraph (i) of Figure 2 show the break strength curves for different  $\gamma$  values at  $\beta=50\%$  and 80%, respectively. From these figures, it can be inferred that at a constant  $\beta$ , the break strength decreases almost linearly from  $\alpha=30^\circ$  to  $90^\circ$ . This could be because an increase in the scratch damage angle reduces the actual tensile area of the geomembrane, effectively reducing its tensile thickness, leading to a decrease in break strength. At  $\alpha=0^\circ$  and  $\beta=50\%$ , the reduction in break strength with depth is significant, while at  $\beta=80\%$ , the decrease is less pronounced.

At  $\alpha=15^\circ$  and  $\beta=50\%$ , the rate of decrease in break strength with depth first diminishes and then increases, while at  $\beta=80\%$ , it gradually increases. At  $\alpha=90^\circ$ , the reduction rate is 52.35% for  $\gamma=50\%$  and 90.66% for  $\gamma=100\%$ , indicating that when the scratch fully penetrates the PVC-P geomembrane, it significantly reduces the break strength.

### 3.2 Elongation at Break

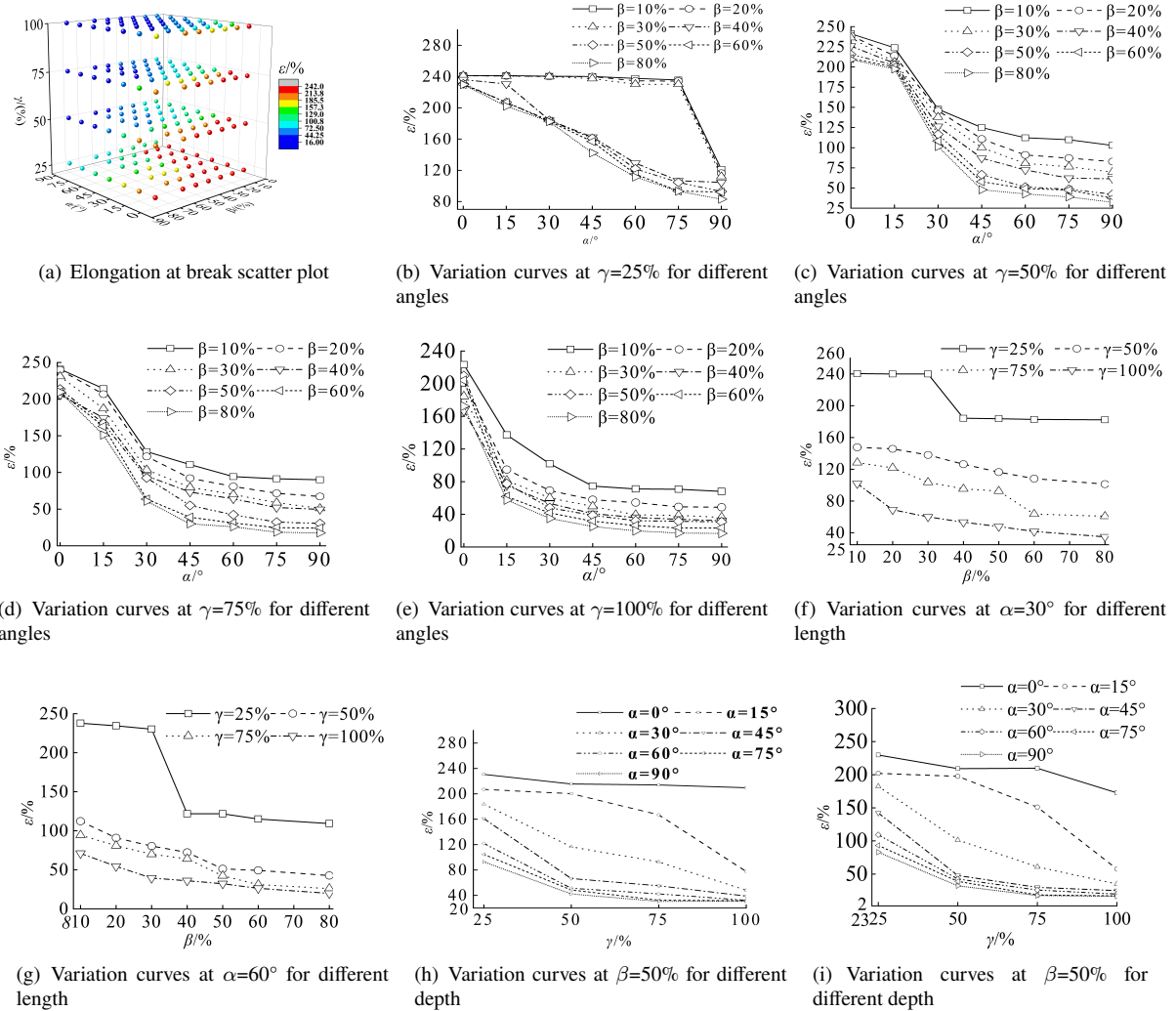


**Figure 3.** Variation of break elongation

Subgraph (a) of Figure 3 presents a three-dimensional scatter plot of the elongation at break ( $\varepsilon$ ) of PVC-P geomembrane specimens with various combinations of scratch damage. The plot reveals a decreasing trend in elongation at break with increasing  $\alpha$ ,  $\beta$ , and  $\gamma$ . This decrease is possibly due to the reduction in the actual area of the specimen subjected to tension, as tearing tends to occur at both ends of the scratch, leading to varying degrees of reduction in elongation at break. Subgraphs (b) through (e) of Figure 3 show the variation curves of elongation at break with changes in  $\alpha$  for four different  $\gamma$  values. At  $\gamma=25\%$ ,  $\beta=10\%-30\%$  shows a minor decrease in elongation at break from  $0^\circ-75^\circ$ , with only a significant drop at  $\alpha=90^\circ$ , while for  $\beta \geq 40\%$ , elongation at break decreases linearly with increasing  $\alpha$ . At  $\gamma=50\%$  and  $75\%$ , the rate of decrease initially increases and then diminishes, with almost no decrease at  $\alpha=75^\circ-90^\circ$ . At  $\gamma=100\%$ , the rate of decrease in elongation at break gradually diminishes as  $\alpha$  increases, with the trend from  $\alpha=45^\circ-90^\circ$  similar to that at  $\gamma=50\%$  and  $75\%$ . Additionally, when  $\beta$  and  $\gamma$  are at their maximum values, the reduction rate at  $\alpha=0^\circ$  is 28.58%, while at  $\alpha=90^\circ$  it reaches 93.12%, indicating that an increase in  $\alpha$  significantly weakens the elongation at break.

Subgraph (f) and Subgraph (g) of Figure 3 illustrate the variation curves of elongation at break with increasing  $\beta$  at  $\alpha=30^\circ$  and  $60^\circ$ , respectively. At  $\gamma=25\%$  and  $\beta=40\%$ , there is a significant drop, while for  $\beta > 40\%$ , the rate of decrease is smaller. For the other three  $\gamma$  values, elongation at break decreases almost linearly with increasing  $\beta$ , and the difference between the maximum and minimum values is smaller than at  $\gamma=25\%$ . At  $\alpha=60^\circ$ , the rate of decrease

is more significant for all four depth ratios with increasing length. For instance, at  $\gamma=100\%$ , the reduction rate is 48.64% at  $\beta=10\%$  and 91.80% at  $\beta=80\%$ . From Subgraph (h) and Subgraph (i) of Figure 3, it can be seen that the elongation at break gradually decreases with increasing  $\gamma$  at both  $\beta=50\%$  and 80%. The rate of decrease is smaller at  $\alpha=0^\circ$ , gradually increasing at  $\alpha=15^\circ$ , and diminishing with increased depth ratio for the other angles. Taking  $\beta=80\%$  as an example, at  $\alpha=90^\circ$ , the reduction rate is 65.66% for  $\gamma=25\%$  and 93.12% for  $\gamma=100\%$ , indicating that an increase in  $\gamma$  also significantly weakens the elongation at break. Overall, scratch damage considerably reduces the elongation at break of PVC-P geomembranes.

## 4 Analysis and Discussion

### 4.1 Three-Factor Variance Analysis

Preliminary analysis of the experimental results on the break strength and elongation at break of scratched PVC-P geomembranes indicates that  $\alpha$ ,  $\beta$ , and  $\gamma$  collectively affect the mechanical properties of PVC-P geomembranes. To more accurately analyze the extent of the influence of these three factors on mechanical properties and their interactions, a multifactorial variance analysis considering interactions is employed. This analysis utilizes the P-value in the F-test to determine the significance of each factor's impact on break strength and elongation at break. A P-value greater than 0.05 suggests that the factor's impact on break strength and elongation at break is not significant, whereas a P-value of 0.05 or less indicates a significant impact. The smaller the P-value, the more significant the impact of the factor. The data were analyzed using the Python programming language, version 3.8.17, with the StatsModels library, specifically the `anova_lm` function. The results of this analysis are presented in Table 2 and Table 3.

**Table 2.** Break strength and three-factor analysis of variance

	<b>df</b>	<b>F</b>	<b>PR (&gt; F)</b>
$\alpha$	6	8216.12	3.78e - 244
$\beta$	7	3561.81	9.32e - 213
$\gamma$	3	12248.65	1.27e - 233
$\alpha \times \beta$	42	27.67	1.63e - 64
$\alpha \times \gamma$	18	274.31	4.21e - 134
$\beta \times \gamma$	21	28.71	4.42e - 50
$\alpha \times \beta \times \gamma$	126	7.86	1.86e - 38

**Table 3.** Break elongation and three-factor analysis of variance

	<b>df</b>	<b>F</b>	<b>PR (&gt; F)</b>
$\alpha$	6	38160.94	2.32e - 313
$\beta$	7	6017.92	2.74e - 236
$\gamma$	3	44068.40	2.88e - 291
$\alpha \times \beta$	42	138.83	2.17e - 130
$\alpha \times \gamma$	18	1712.69	3.78e - 215
$\beta \times \gamma$	21	272.69	6.46e - 139
$\alpha \times \beta \times \gamma$	126	63.79	3.61e - 121

Table 2 and Table 3 present the results of the three-factor variance analysis for break strength and elongation at break. The analysis of each single factor  $\alpha$ ,  $\beta$ , and  $\gamma$  yielded a P-value less than 0.05, indicating that all three factors significantly affect both break strength and elongation at break. Among these, the factor  $\alpha$  has the smallest P-value, suggesting that the scratch angle has the most significant impact on the mechanical properties of PVC-P geomembranes. The interaction between the two factors  $\alpha$  and  $\gamma$  showed the most significant impact on both the break strength and elongation at break of PVC-P geomembranes. Although the P-values for the interactions of other pairs of factors were higher than for the  $\alpha$  and  $\gamma$  interaction, their impacts were also significant. Additionally, the P-values for all three dual-factor interactions were higher than for any single factor, indicating that the impact of dual-factor interactions is less than that of single factors. The results of the three-factor variance analysis also showed P-values less than 0.05, but these were still higher than the P-values for single and dual factors. This suggests that the combined interaction of the three factors has a less significant impact on the break strength and elongation at break of PVC-P geomembranes compared to single factors. In conclusion, the interactions between two and three factors reduce the extent of the impact exerted by single factors.

## 4.2 Multivariate Regression Analysis

To construct a regression model correlating the mechanical properties of PVC-P geomembranes with  $\alpha$ ,  $\beta$ , and  $\gamma$ , it is necessary to analyze the relationship between these three factors and both break strength and elongation at break. For this, the Pearson correlation coefficient method was used within the programming environment. Values for  $\alpha$ ,  $\beta$ , and  $\gamma$ , as well as the rates of decrease in break strength and elongation at break, were imported into Python, and the `corr()` method was called to calculate the correlation coefficients between columns. By specifying the “method=Pearson” parameter, the computation for the Pearson correlation coefficient method was carried out. The results are stored in ‘correlations’ and represented in the form of a heatmap (as shown in Figure 4). According to the heatmap, it is evident that the break strength ( $T$ ) and elongation at break ( $\varepsilon$ ) have a high correlation with  $\alpha$ ,  $\beta$ , and  $\gamma$ , all showing negative correlations. This indicates that an increase in  $\alpha$ ,  $\beta$ , and  $\gamma$  leads to a decrease in the mechanical properties of the PVC-P geomembrane, which is consistent with the experimental analysis results. Additionally, the correlation coefficients between any two of  $\alpha$ ,  $\beta$ , and  $\gamma$  are non-zero, suggesting the presence of interaction effects between any two of these factors. Therefore, interaction terms should be included in the regression model to accurately reflect these dynamics.

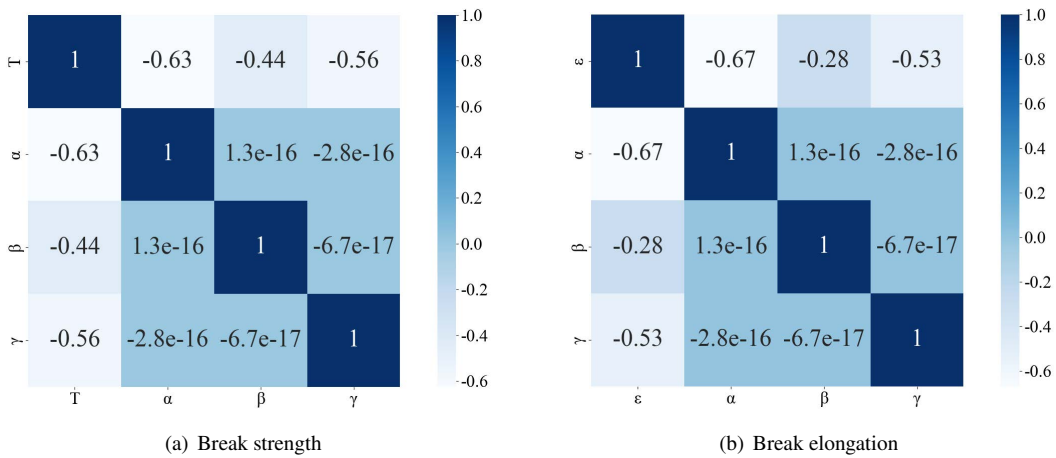


**Figure 4.** Break strength and break elongation and scratch damage three factors correlation coefficient diagram

Based on the analysis, multivariate regression equations can be established to relate the break strength and elongation at break of PVC-P geomembranes with the three factors ( $\alpha$ ,  $\beta$ , and  $\gamma$ ). The equations are presented as Eq. (4) for break strength and Eq. (5) for elongation at break:

$$T_p = a_0 + a_1\alpha + a_2\beta + a_3\gamma + a_4\alpha^2 + a_5\beta^2 + a_6\gamma^2 + a_7\alpha^3 + a_8\beta^3 + a_9\gamma^3 + a_{10}\alpha^2\beta + a_{11}\alpha\beta^2 + a_{12}\alpha^2\gamma + a_{13}\alpha\gamma^2 + a_{14}\beta^2\gamma + a_{15}\beta\gamma^2 + a_{16}\alpha\beta + a_{17}\alpha\gamma + a_{18}\beta\gamma + a_{19}\alpha\beta\gamma \quad (4)$$

$$\varepsilon_p = b_0 + b_1\alpha + b_2\beta + b_3\gamma + b_4\alpha^2 + b_5\beta^2 + b_6\gamma^2 + b_7\alpha^3 + b_8\beta^3 + b_9\gamma^3 + b_{10}\alpha^2\beta + b_{11}\alpha\beta^2 + b_{12}\alpha^2\gamma + b_{13}\alpha\gamma^2 + b_{14}\beta^2\gamma + b_{15}\beta\gamma^2 + b_{16}\alpha\beta + b_{17}\alpha\gamma + b_{18}\beta\gamma + b_{19}\alpha\beta\gamma \quad (5)$$

**Table 4.** Regression coefficient of break strength model

Coefficient	Value	Coefficient	Value
$a_0$	29.78	$a_{10}$	0.001
$a_1$	0.175	$a_{11}$	0.168
$a_2$	23.097	$a_{12}$	0.005
$a_3$	-20.477	$a_{13}$	0.257
$a_4$	-0.001	$a_{14}$	15.013
$a_5$	-64.737	$a_{15}$	10.553
$a_6$	45.41	$a_{16}$	-0.279

In these equations,  $T_p$  and  $\varepsilon_p$  represent the predicted values of break strength and elongation at break, respectively, as estimated by the regression model. For this experiment, a test set of 184 randomly selected data points was used, with 12 of these serving as the test set. The coefficients  $a_0 - a_{19}$  and  $b_0 - b_{19}$  are the model fitting coefficients, where

$a_0 - a_3$  and  $b_0 - b_3$  control the linear variation of the model, while  $a_4 - a_{19}$  and  $b_4 - b_{19}$  control the non-linear variation. The 184 data points were imported into the SPSS software for analysis to determine the values of each coefficient. The version of the SPSS software used was IBM SPSS Statistics 26. The values for  $\alpha$ ,  $\beta$ , and  $\gamma$ , and the attenuation rates were imported into the software, and the non-linear regression analysis was conducted using the ‘Analyze-Regression-Nonlinear’ option. Eqs. (4) and (5) were entered into the formula box, along with all the fitting coefficients. The analysis provided the various fitting parameters, with detailed results presented in Table 4 and Table 5.

**Table 5.** Regression coefficient of break elongation model

Coefficient	Value	Coefficient	Value
$b_0$	376.865	$b_{10}$	0.026
$b_1$	2.11	$b_{11}$	0.849
$b_2$	-64.238	$b_{12}$	0.057
$b_3$	-681.709	$b_{13}$	4.67
$b_4$	0.001	$b_{14}$	-42.005
$b_5$	-93.785	$b_{15}$	-82.042
$b_6$	1155.87	$b_{16}$	-4.918
$b_7$	0.000	$b_{17}$	-11.807
$b_8$	140.991	$b_{18}$	121.384
$b_9$	-644.452	$b_{19}$	1.859

Based on Table 4 and Table 5, the regression model expressions for break strength and elongation at break can be represented as Eq. (6) for break strength and Eq. (7) for elongation at break.

$$T_P = 29.78 + 0.175\alpha + 23.097\beta - 20.477\gamma - 0.001\alpha^2 - 64.737\beta^2 + 45.41\gamma^2 + 41.629\beta^3 - 30.938\gamma^3 + 0.001\alpha^2\beta + 0.168\alpha\beta^2 + 0.005\alpha^2\gamma + 0.257\alpha\gamma^2 + 15.013\beta^2\gamma + 10.553\beta\gamma^2 - 0.279\alpha\beta - 0.79\alpha\gamma - 26.286\beta\gamma - 0.056\alpha\beta\gamma \quad (6)$$

$$\varepsilon_P = 376.865 + 2.11\alpha - 64.238\beta - 681.709\gamma + 0.001\alpha^2 - 93.785\beta^2 + 1155.87\gamma^2 + 140.991\beta^3 - 64.4522\gamma^3 + 0.026\alpha^2\beta + 0.849\alpha\beta^2 + 0.057\alpha^2\gamma + 4.67\alpha\gamma^2 - 42.005\beta^2\gamma - 82.04 + 2\beta\gamma^2 - 4.918\alpha\beta - 11.807\alpha\gamma + 121.384\beta\gamma + 1.859\alpha\beta\gamma \quad (7)$$

Using Eqs. (6) and (7), the break strength and elongation at break for 12 different combinations were predicted. Figure 5 and Figure 6 illustrate the predictive accuracy of the regression models for break strength and elongation at break under these 12 combinations, with  $R^2$  values of 0.98 and 0.97, respectively. Figure 7 shows the relative errors between the predicted values of the regression model and the experimental values. The MAPE for these models are 3.06% and 5.13%, respectively, while the MAE is 0.62 kN/m for break strength and 7.96% for elongation at break. The RMSE is 0.84 kN/m for break strength and 12.08% for elongation at break. These results demonstrate that the two regression models can accurately describe the relationship between the break strength and elongation at break of PVC-P geomembranes and the factors  $\alpha$ ,  $\beta$ , and  $\gamma$ .

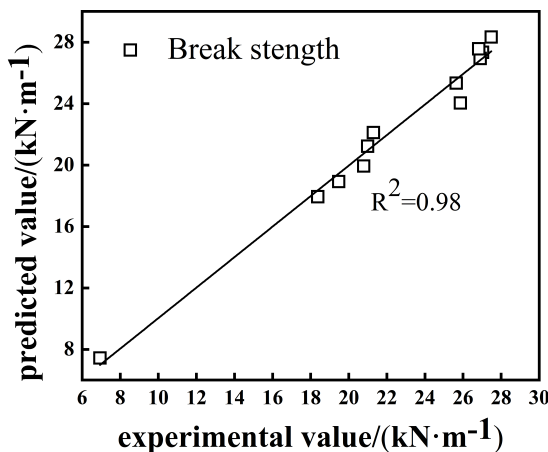


**Figure 5.** Break strength model data fitting

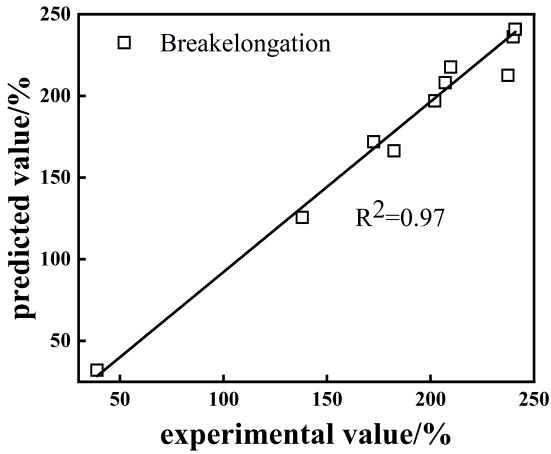


**Figure 6.** Break elongation model data fitting

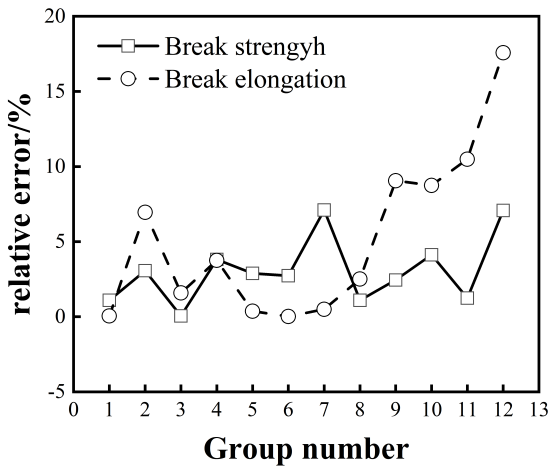


**Figure 7.** Relative error of two models

It should be noted that the models constructed are specifically for assessing the mechanical performance degradation due to scratch damage in PVC-P geomembranes. In practical engineering applications, when scratch damage occurs in PVC-P geomembranes, these models can accurately predict changes in mechanical properties. These predictions can then be compared and analyzed against the allowable values stipulated in the technical specifications for the use of geosynthetic materials. This assessment helps in determining whether the mechanical properties of scratched PVC-P geomembranes meet.

## 5 Conclusions

This paper conducted axial tensile mechanical tests on PVC-P geomembranes with various combinations of scratch angle, length, and depth. Based on the experimental results, regression analysis models were constructed, and the congruence between the model predictions and experimental values was analyzed. The main conclusions are as follows:

(1) Scratch damage significantly weakens the axial tensile mechanical properties of PVC-P geomembranes, with the most pronounced reduction in elongation at break. In practical engineering, efforts should be made to minimize the possibility of scratch damage to PVC-P geomembranes. It is recommended to improve construction techniques and refine construction methods, such as avoiding human and mechanical disturbances during geomembrane installation and designing appropriate particle gradation curves for subgrade layers.

(2) The mechanical properties of PVC-P geomembranes are significantly influenced by the interaction of scratch angle, length, and depth, among which the scratch angle has the most significant impact. This aspect should be given attention during construction.

(3) A multivariate regression analysis model for the break strength and elongation at break of scratched PVC-P geomembranes has been developed. This model is specific to PVC-P geomembranes and can provide a reference for assessing the mechanical performance of geomembranes with scratch damage.

## 6 Works in the Future

Although the model constructed in this paper can determine the degree of mechanical performance degradation in PVC-P geomembranes with varying degrees of scratch damage, it is not convenient for practical engineering applications. Therefore, future research should focus on developing a method to accurately assess the mechanical performance of scratched PVC-P geomembranes and determine threshold values for scratch damage in terms of angle, length, and depth that affect the mechanical properties of PVC-P geomembranes.

## Funding

This paper was funded by the National Natural Science Foundation of China (Grant No.: 516069087); the National Natural Science Foundation of China (Grant No.: 51709114).

## Data Availability

The data used to support the findings of this study are available from the corresponding author upon request.

## Conflicts of Interest

The authors declare that they have no conflicts of interest.

## References

- [1] Y. Ning, J. Q. Yu, and L. J. Cui, “Anti-seepage of geomembrane for high soft rock filling dam,” *Water Power*, vol. 42, no. 5, pp. 62–67, 2016. <https://doi.org/10.3969/j.issn.0559-9342.2016.05.017>
- [2] X. Xia, H. Y. Qiu, X. K. Xie, Z. G. Gao, J. X. Chen, and W. W. Zhang, “The influence of geomembrane liner on the stability of landfill at different ages,” *Chin. J. Environ. Eng.*, vol. 16, no. 10, pp. 3417–3422, 2022. <https://doi.org/10.12030/j.cjee.202202094>
- [3] R. K. Rowe, “Performance of GCLs in liners for landfill and mining applications,” *Environ. Geotech.*, vol. 1, no. 1, pp. 3–21, 2014. <https://doi.org/10.1680/envgeo.13.00031>
- [4] A. Scuero and G. Vaschetti, “Geomembrane sealing systems for dams: ICOLD Bulletin 135,” *Innov. Infrastruct. Solut.*, vol. 2, pp. 1–17, 2017. <https://doi.org/10.1007/s41062-017-0089-0>
- [5] Y. M. Shu, “Progress in geomembrane barriers for seepage prevention in reservoirs and dams in China,” *Adv. Sci. Technol. Water Resour.*, vol. 35, no. 5, pp. 20–26, 2015. <https://doi.org/10.3880/j.issn.10067647.2015.05.003>
- [6] J. P. Giroud and K. L. Soderman, “Comparison of geomembranes subjected to differential settlement,” *Geosynth. Int.*, vol. 2, no. 6, pp. 953–969, 1995. <https://doi.org/10.1680/gein.2.0043>
- [7] Y. M. Shu, H. M. Wu, X. Z. Jiang, and K. Gu, “Mechanism of anchoring influence at perimeter of high membrane faced rockfill dam and eliminating approach: key technology of high membrane faced rockfill dam (II),” *Adv. Sci. Technol. Water Resour.*, vol. 5, no. 1, pp. 10–15, 2015. <https://doi.org/10.3880/j.issn.10067647.2015.01.002>
- [8] X. L. Zhang, Y. F. Liu, K. Gu, and W. L. Mao, “Experimental study on geomembrane bending (folding) in anti-seepage structure of membrane-faced rockfill dam,” *Chin. J. Geotech. Eng.*, vol. 41, no. 8, pp. 555–1561, 2019. <https://doi.org/10.11779/CJGE201908021>
- [9] K. Peng, Y. G. Yin, G. H. Wang, and H. G. Ou, “Application of geomembrane in Jiangpinghe hydropower station project,” *Water Power*, vol. 46, no. 6, pp. 53–56, 2020. <https://doi.org/10.3969/j.issn.0559-9342.2020.06.013>
- [10] E. M. Gallagher, D. M. Tonks, J. Shevelan, A. R. Belton, and R. E. Blackmore, “Investigations of geomembrane integrity within a 25-year old landfill capping,” *Geotext. Geomembr.*, vol. 44, no. 5, pp. 770–780, 2016. <https://doi.org/10.1016/j.geotexmem.2016.05.011>
- [11] J. P. Giroud and N. Morel, “Analysis of geomembrane wrinkles,” *Geotext. Geomembr.*, vol. 11, no. 3, pp. 255–276, 1992. [https://doi.org/10.1016/0266-1144\(92\)90003-S](https://doi.org/10.1016/0266-1144(92)90003-S)
- [12] D. Narejo, R. M. Koerner, and R. F. Wilson-Fahmy, “Puncture protection of geomembranes Part II: Experimental,” *Geosynth. Int.*, vol. 3, no. 5, pp. 629–653, 1996. <https://doi.org/10.1680/gein.3.0078>
- [13] T. D. Stark, T. R. Boerman, and C. J. Connor, “Puncture resistance of PVC geomembranes using the truncated cone test,” *Geosynth. Int.*, vol. 15, no. 6, pp. 480–486, 2008. <https://doi.org/10.1680/gein.2008.15.6.480>
- [14] G. M. Xu, W. M. Zhang, and G. X. Peng, “Effect of damage on mechanical behavior of HDPE geomembrane,” *J. Hohai Univ. (Nat. Sci.)*, vol. 2004, no. 1, pp. 76–80, 2004. <https://doi.org/10.3321/j.issn:1000-1980.2004.01.018>
- [15] R. K. Rowe and J. Fan, “Effect of geomembrane hole geometry on leakage overlain by saturated tailings,” *Geotext. Geomembr.*, vol. 49, no. 6, pp. 1506–1518, 2021. <https://doi.org/10.1016/j.geotexmem.2021.06.004>
- [16] W. J. Cen, K. Bolanhan, and F. R. Liu, “Experimental study on tensile properties of defective and damaged geomembrane,” *Adv. Sci. Tech. Water Res.*, vol. 41, no. 1, pp. 69–73, 2021. <https://doi.org/10.3880/j.issn.1006-7647.2021.01.011>

- [17] X. L. Zhang, Z. Y. Ma, and Y. Y. Wu, "Mechanical properties of different geomembranes in membrane-faced rockfill dam," *Chin. J. Geotech. Eng.*, vol. 45, no. 5, pp. 940–952, 2023. <https://doi.org/10.11779/CJGE20220151>
- [18] H. Chen, G. L. Zhou, J. Yan, Y. Ji, and C. M. Yan, "Study on particle matching algorithm for surface flow field based on regression analysis," *Adv. Sci. Tech. Water Res.*, vol. 40, no. 1, pp. 32–36, 2020. <https://doi.org/10.3880/j.issn.1006-7647.2020.01.005>
- [19] Q. Wang, T. T. Zhang, H. L. You, J. Chang, and Y. Q. Cao, "Mid-long term runoff forecasting model for Dahuofang reservoir based on multiple regression analysis," *Water Power*, vol. 40, no. 5, pp. 17–20, 2014. <https://doi.org/10.3969/j.issn.0559-9342.2014.05.005>
- [20] L. J. Zhou, L. M. Xing, L. L. Bai, H. Yang, S. W. Quan, and E. X. Xiang, "Fault characteristics of XLPE cable terminal ring damage based on multiple nonlinear regression model," *High Volt. Eng.*, vol. 47, no. 9, pp. 3124–3133, 2021. <https://doi.org/10.13336/j.1003-6520.hve.20200829>
- [21] Ministry of Water Resources, *Specification for Test and Measurement of Geosynthetics: SL235-2012*. China Water & Power Press, Beijing, 2012.